ASTRONOMY METHODS

A Physical Approach to Astronomical Observations

HALE BRADT
Massachusetts Institute of Technology

CAMBRIDGE
UNIVERSITY PRESS

PUBLISHED BY THE PRESS SYNDICATE OF THE UNIVERSITY OF CAMBRIDGE
The Pitt Building, Trumpington Street, Cambridge, United Kingdom

CAMBRIDGE UNIVERSITY PRESS
The Edinburgh Building, Cambridge CB2 2RU, UK
40 West 20th Street, New York, NY 10011-4211, USA
477 Williamstown Road, Port Melbourne, VIC 3207, Australia
Ruiz de Alarcón 13, 28014 Madrid, Spain
Dock House, The Waterfront, Cape Town 8001, South Africa

http://www.cambridge.org

First published 2004

Printed in the United Kingdom at the University Press, Cambridge

Typefaces Times 11/14 pt. and Univers *System* LaTeX 2$_\varepsilon$ [TB]

A catalog record for this book is available from the British Library

Library of Congress Cataloging in Publication data
Bradt, Hale, 1930–
Astronomy methods: a physical approach to astronomical observations / Hale Bradt.
p. cm.
Includes bibliographical references and index.
ISBN 0 521 36440 X – ISBN 0 521 53551 4 (pbk.)
1. Astronomy. I. Title.
QB45.2.B73 2003 520–dc21 2002041703

ISBN 0 521 36440 X hardback
ISBN 0 521 535514 paperback

Contents

Figures

Tables

5

Telescopes

What we learn in this chapter

Telescopes and **antennas** collect photons, and the detectors at their foci record the information content of the radiation, its **intensity** and **polarization** as a function of time, and also its **frequency distribution** and **direction of arrival**. There are several common **configurations of optical telescopes**. **Focal length** and **aperture** determine the **plate scale**, **sensitivity** and potential **resolution** of the telescope. **Non-focusing** instruments are used by **gamma-ray astronomers** while **x-ray astronomers** use both focusing and non-focusing systems. Telescope resolution may be limited by **diffraction**. The **point-spread function** describes the shape of the (single pixel) telescope **beam**. The resolution of large ground-based optical telescopes is severely limited by **non-planar wavefronts** caused by atmospheric turbulence. **Speckle interferometry and adaptive optics** are techniques for overcoming this limitation.

5.1 Introduction

The systems that extract information from faint signals about distant celestial bodies are the source of essentially all our astronomical knowledge. Telescopes collect and concentrate the radiation, and the instruments at their foci analyze one or more properties of the radiation. The systems used for the various frequency bands (e.g., radio, optical, and x-ray) differ dramatically from one another.

The faint signals must compete with background noise from the cosmos, the atmosphere, the earth's surface, and the detectors themselves. These noise sources differ with the frequency of the radiation. Advances in astronomy often follow from improved rejection of noise so that fainter signals can be detected. For example, improved focusing yields a smaller spot on the image plane (film or CCD), and the

signal need only compete with the smaller amount of instrument noise occurring at this smaller region.

In this chapter, we present some characteristics of telescopes including their focusing properties. The diffraction phenomenon that can limit the resolution of telescopes is described. Current efforts to develop systems to remove the blurring due to the atmosphere are also discussed. In the following chapter we describe detectors that are placed at the foci of the telescopes.

5.2 Information content of radiation

All astronomical telescope and detector systems have the same purpose, namely, the study of incoming photons with the maximum possible sensitivity, and with the optimum frequency, timing, and angular resolution. One can not always attain the best possible performance in all these aspects at the same time.

A stellar object at a great ("infinite") distance appears to us as a "point" source; its angular size is smaller than is resolvable by our eye or instrument. Light rays may diverge isotropically from it, but at the great distance of our telescope, the small subset of rays impinging on it is effectively parallel. The beam of photons arriving at the earth is thus like rain falling everywhere parallel to itself. In terms of waves, the wavefronts are everywhere normal to the propagation direction. This signal from a point-like source is called a plane wave.

Telescopes capture the portion of the incoming energy that impinges on the telescope aperture. A larger telescope can collect more energy (rain) each second. The instruments on the telescope are used to determine the properties of the collected electromagnetic radiation (or incoming photons). The properties that can be measured are limited in number. They are:

(*i*) The rate (number per unit time) of arriving photons. This rate follows from the total power radiated by the source of the radiation, the average energy of the individual photons, and the distance to the source. (At radio frequencies one measures the amplitude of the electromagnetic wave in lieu of counting photons.) This rate can vary with time, for example from variable stars and pulsars. The former variations arise from periodic changes in radius and brightness of a star, while the latter arise from the rotation of a neutron star.

(*ii*) The arrival directions of the photons, or equivalently, the regions of the sky from which they originate. This allows one to describe the angular shape of the source on the sky. The photon numbers and energies from different directions determine, for example, the brightness distribution of a diffuse nebula.

(*iii*) The photon energy $h\nu$ (or equivalently the frequency or wavelength) of the radiation. This allows one to determine how the incoming radiation is distributed in frequency (the *spectrum*). For example, a concentration of energy at one frequency

(a *spectral line*) would indicate the existence of a particular atom, such as hydrogen, undergoing a specific atomic transition. The existence of such transitions gives information about the temperatures and densities in the atmospheres of stars as well as their speeds from Doppler shifts of the frequency.

(*iv*) The polarization, i.e., the directions of the transverse electric vector $\boldsymbol{E}$ of the incoming electromagnetic wave. A predominance of vectors in one direction is indicative of polarized light. This can indicate, for example, that the emitting particles (electrons) are significantly influenced by magnetic fields in the emitting region or that the light has been scattered by dust grains in the interstellar medium.

The sensitivity or precision with which a given telescope–detector system is able to measure these quantities is crucial to understanding the data obtained with it. For example, the angular resolution is the capability of the system to distinguish (or resolve) two adjacent objects, expressed as the minimum separation angle. This is typically $1''$ for a ground-based optical telescope, about $0.05''$ for a large space-borne optical telescope (e.g., the Hubble Space Telescope), and better than $0.001''$ for several radio telescopes operating together from locations on different continents.

Similarly, frequency resolution is the ability to distinguish two spectral lines at closely adjacent frequencies. High-dispersion, *echelle-grating spectrometers* used on optical telescopes attain resolutions in wavelength of $\Delta\lambda \lesssim 0.10$ nm. Since the wavelength of optical radiation is $\sim$500 nm, the *resolution*, defined as $\lambda/\Delta\lambda$, is $\sim$5000. Timing resolution is the ability of the instrument to distinguish the arrival times of single photons (or groups of photons) that arrive at closely spaced times. Pulses of radio emission arrive from spinning neutron stars with separations as small as 1.6 ms.

5.3 Image formation

Telescopes and antennas are the light collectors of astronomy. They come in varying shapes and sizes that depend in part on the frequency of radiation they are designed to detect. Most systems concentrate the incoming radiation by means of *focusing*. Optical telescopes gather light with a lens or a reflecting surface (a mirror). Radio telescopes make use of reflecting metal surfaces. X-ray telescopes make use of the reflecting character of a smooth metal surface for x rays impinging on it at a low glancing ("grazing") angle, like a stone skipping on water. Some radio and x-ray detection systems and all gamma-ray systems do not focus the radiation. These are non-focusing systems.

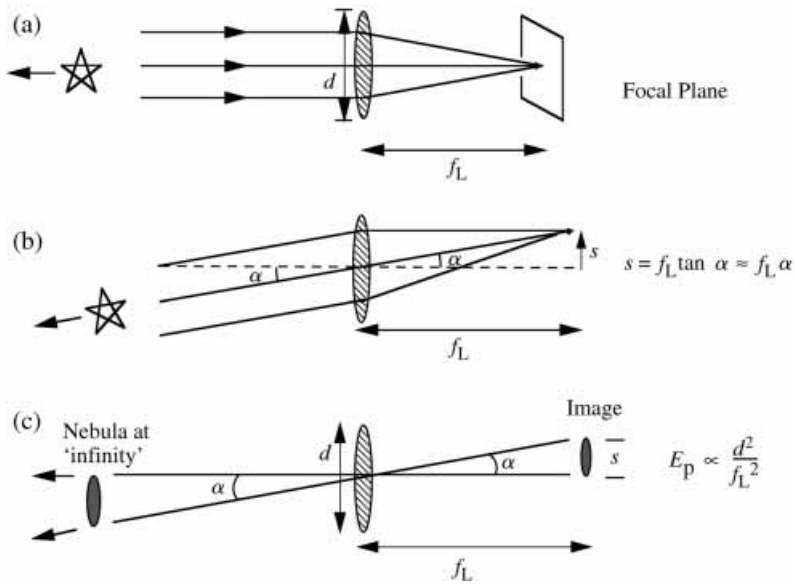

Figure 5.1. The focusing characteristics of an ideal thin lens. The focal length f_L and the aperture d are each measured in meters. (a) Parallel beam arriving along the lens axis, and focusing at distance f_L. (b) Off-axis parallel beam (small angle α) also converging at distance f_L, but displaced a distance $s = f_L \tan\alpha$ from the lens axis. (c) Extended source subtending angle α and depositing, in a fixed time, energy $E_p \propto (d/f_L)^2$ onto a single pixel of the image plane.

Focusing systems

Focal length and plate scale

The radiation from a very distant point-like star arrives at earth as a parallel beam of light. If the light impinges normally onto a thin (ideal) convex lens (Fig. 1a), a parallel bundle of rays will focus to an on-axis point image in the *focal plane*, a distance f_L (*focal length*) beyond the lens. If the parallel rays arrive at an angle α from the lens axis, they will also focus to a point in the focal plane (Fig. 1b), but at a distance s removed from the optical axis. The vertical position of the focus is defined by the ray that passes through the center of the lens; it will transit the (thin) lens without being deviated. The relation between these quantities is

$$s = f_L \tan\alpha \underset{\alpha \text{ small}}{\longrightarrow} f_L\, \alpha \qquad \text{(m)} \qquad (5.1)$$

This geometry can also be applied to a properly figured concave mirror (or system of mirrors) that brings a parallel beam of light to a focus.

If there were two stars, one on axis and the other off axis as shown in Figs. 1a,b, they would be separated in the sky by the angle α and on the plate by the

distance s. The relation (1) gives the star separation in the focal plane, or on a photographic plate exposed in the focal plane. A nebula with angular diameter α (Fig. 1c) would have this same diameter s on the photograph. A large focal length yields a large star separation or nebular image, and a small focal length yields a small image. A small focal length requires the lens or mirror to refract the rays more strongly (Fig. 1a), and this leads to difficulties of design and limitations in performance (e.g., depth and breadth of the well-focused region). On the other hand, such a telescope can fit inside a smaller, and hence cheaper, telescope building.

The *plate scale* describes the angle that is imaged onto unit length of the plate; it is simply the ratio of α and s which is the inverse of the focal length,

$$P_{\mathrm{s}} = \frac{\alpha}{s} = \frac{1}{f_{\mathrm{L}}} \qquad \text{(rad/m; plate scale)} \qquad (5.2)$$

The units are m^{-1} or, equivalently, radians/meter; radians have no dimension. A large plate scale means the image size s is small and vice versa. In practice, the plate scale is usually given in "arcsec per mm" ($''$/mm). The focal length of the Lick 3-m (diameter) telescope is $f_{\mathrm{L}} = 15.2$ m giving a plate scale of $14''$/mm at the prime focus. A 1° piece of the sky would occupy a full $1/4$ m in the focal plane. A given telescope may offer a choice of several focal lengths, for example by changing the *secondary mirror* (see below).

Aperture and deposited energy

The rate of energy deposited on a single grain of film, or on the single pixel of a modern electronic imaging device, determines whether a given incident energy flux can be detected in a given time. A large telescope aperture (diameter d) will increase the energy flow onto the detector because a larger part of the incoming wavefront is intercepted and focused. For a perfect point source, perfect atmosphere, and perfect lens, all the collected photons from a source will be deposited onto the same grain of the film or the same pixel of an electronic detector. In this ideal case, the aperture alone determines the needed exposure; the focal length does not enter.

However, if the celestial source has a significant finite angular size, like the moon or a nebula, the energy will be deposited over a number of grains or pixels (Fig. 1c). If the image is spread over a large number of pixels because of a large focal length, a longer exposure is required to obtain a detectable signal in a given pixel. If, in contrast, the image is concentrated in a small region because of a short focal length, there is more energy deposited in a given pixel in a given time. In this case, the source image appears smaller but is more quickly detected.

The area of a circular image of diameter s is proportional to s^2. Thus, for a nebula of (fixed) angular size α, the energy deposited onto a single pixel for a

fixed telescope mirror aperture is $E_{\rm p} \propto s^{-2} \propto f_{\rm L}^{-2}$ where we used $s \propto f_{\rm L}$ from (1). Also, a larger aperture will allow more photons to be collected proportionally to the collecting area a of the mirror where $a \propto d^2$. Thus, for diffuse sources, the energy deposited per unit time onto a single pixel depends on both the aperture and the focal length,

$$\Rightarrow \qquad E_{\rm p} \propto \left(\frac{d}{f_{\rm L}}\right)^2 \qquad \text{(Energy per unit time onto single pixel)} \qquad (5.3)$$

The ratio $f_{\rm L}/d$ is called the *focal ratio*,

$$\Re \equiv \frac{f_{\rm L}}{d} \qquad \text{(Focal ratio)} \qquad (5.4)$$

From (3) and (4) it is apparent that the focal ratio is an inverse measure of how fast energy is deposited on an element of the image plane. One refers to the "speed" of the optical system; it is proportional to the energy $E_{\rm p}$ deposited in a given time. Thus, speed $\propto E_{\rm p} \propto \Re^{-2}$. A greater speed means a photograph or other measurement may be carried out in less time.

The *focal ratio* is usually indicated with the notation "$f/\Re$"; i.e., a focal ratio of 6 is written "$f/6$", when, in fact, it is the aperture d which is equal to $f_{\rm L}/\Re$; see (4). When you see "$f/6$", think "$\Re = 6$, the focal length $f_{\rm L}$ is 6 times the aperture d". Amateur cameras usually have a focal ratio adjustment which can be varied from about $f/2$ to about $f/16$. This is accomplished by changing the aperture with an adjustable diaphragm; the focal length does not change. A "50-mm lens" refers to the focal length $f_{\rm L}$. Zoom lenses change the focal length.

The speed of an optical system depends only on the ratio $\Re$; it is independent of the specific camera used. A 1-m telescope with $f/6$ optics will be just as fast as a 4-m system with $f/6$ optics. Less light is collected by the smaller 1-m aperture, but the focal length is also shorter. This causes the energy to be concentrated onto a smaller area in the image plane. Thus the energy deposited per pixel remains the same for the two systems. Slower optics (greater $\Re$) are sometimes desirable; the image is more spread out (greater magnification) and the angular resolution is improved. But it takes longer to get a good exposure.

A special kind of telescope design, the *Schmidt telescope* uses a refracting corrector plate in front of the principal (primary) mirror to produce high quality images over a large $5^\circ \times 5^\circ$ angular field. It features a short focal length. The focal ratio for the large Palomar Schmidt telescope is $\Re = 2.5$. The short focal length yields low magnification causing a lot of energy to be focused onto each pixel. The Schmidt design is thus very fast. It was the ideal instrument to make the Palomar Observatory Sky Survey described in Section 3.4.

Telescope configurations

Optical light may be collected and focused by means of a transmitting lens that refracts the rays as shown in Figs. 1a and 2a. The disadvantage of a lens in astronomy is that the light must traverse the glass which can lead to imperfect focusing due for example to color dependence of the index of refraction (*chromatic aberration*). Also, the lenses become very heavy as they become larger. This makes difficult the precision positioning and support of the lens in a movable telescope structure as is required for a good focus. In contrast, a relatively lightweight mirror may be used to reflect the light to a focus (Fig. 2b). In this case it is only the shape of the mirror that must be precisely machined and maintained. All current major optical telescopes use reflective optics.

A *primary mirror* concentrates the light at a *primary focus* (Fig. 2b). For the very largest telescopes, instruments can be mounted at the primary focus and an astronomer can ride around in a little cage which surrounds the focus. This allows her to change photographic plates, all the time listening to classical music, seemingly suspended among the stars. We say "ride" because the telescope will point to many different positions in the sky on a typical night of observing. Unfortunately, modern electronic detectors generally make such rides unnecessary now. Most radio telescopes operate in the prime-focus configuration. They often feature a large metallic antenna dish that reflects the radiation to a detector at the prime focus.

Alternatively, a *secondary mirror* can direct the light through a hole in the large primary mirror to the *Cassegrain focus* (Fig. 2c). The secondary mirror blocks some of the light entering the telescope, but only a small fraction of it. The Cassegrain focus is convenient because large, heavy instruments can be mounted more easily on the back end of the telescope. The secondary mirror can be changed to modify the effective focal length in many telescopes. One practice is for the secondary-mirror structure to contain two mirrors (Fig. 2c). Rotation of the secondary mirror structure by 180° moves the alternate mirror into the beam.

The light from the primary mirror can be intercepted by a flat mirror which directs the light toward the side of the telescope to the *Newtonian focus* which can be examined with an eyepiece mounted on the side of the telescope (Fig. 2d). This scheme is often used for amateur telescopes. In large telescopes, the light can be directed by a series of mirrors to a temperature-controlled room below the telescope to the *Coudé focus* (not shown). There a large spectroscope disperses the light into its spectral colors with high resolution (large $\lambda/\Delta\lambda$).

Traditionally optical telescopes are mounted with two orthogonal axes of rotation, one polar (pointing to the celestial pole), called a *polar mount*; see "Why equatorial coordinates?" in Section 3.2. Radio telescopes and new larger optical telescopes

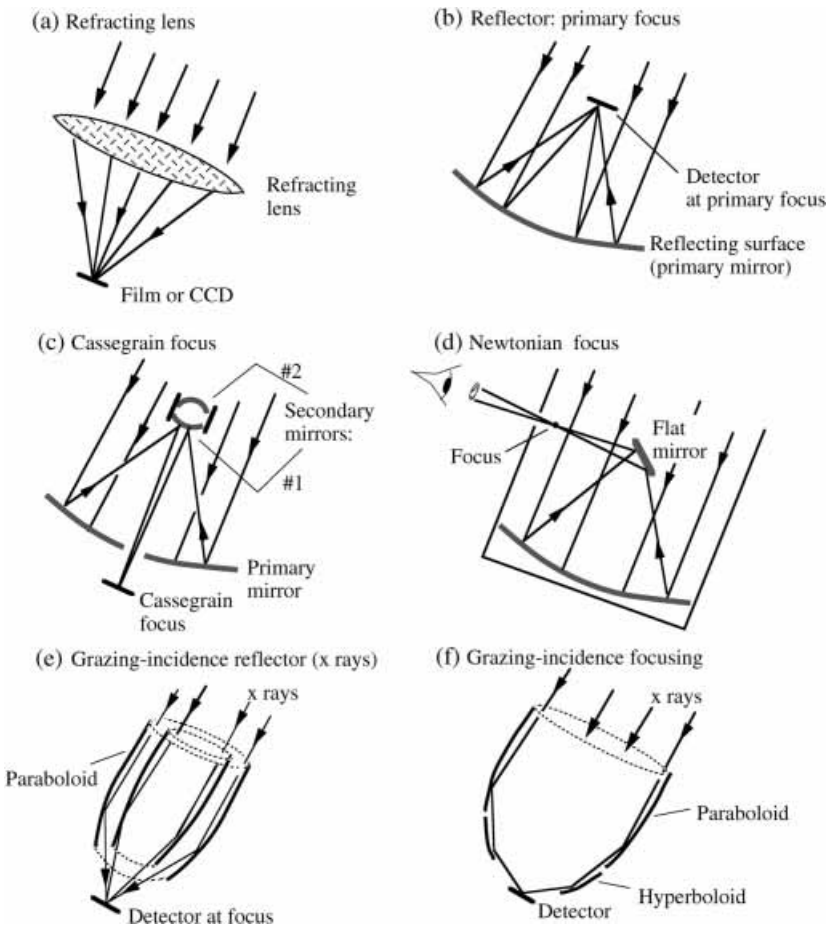

Figure 5.2. Focusing systems. (a) Refracting lens. (b,c,d) Reflecting telescope with primary focus, Cassegrain focus, and Newtonian focus, respectively. The choice of two secondary mirrors in a given telescope allows the telescope to operate with two different focal lengths. (e,f) Grazing incidence x-ray telescopes with one reflection and two reflections. Additional collecting area can be obtained by nesting the mirrors as shown in (e). The foci shown here are unrealistically close to the collectors.

are often mounted in the *altitude-azimuth* configuration where one axis or rotation is horizontal and the other vertical. This simplifies the mechanical design and makes it easier to keep the primary mirror in its optimal shape. It is easily distorted by thermal gradients and the varying forces of gravity as the telescope moves to new orientations. The newest optical telescopes have sophisticated systems for monitoring and adjusting the shape of the primary mirror so that it can be kept in its optimal shape throughout a night of observing.

Telescope designs also pay great attention to keeping thermal gradients and convection to a minimum. Unknown to astronomers for a century was the fact that thermal currents within the telescope building were a major source of poor image quality. This arose from solar heating of concrete structures that are slow to cool and to power dissipation in the building (heated offices, etc.) The Magellan/Baade telescope in Chile is obtaining images as good as $0.30''$ (full-width at half maximum intensity) with good thermal and mirror-shape control.

The grazing incidence arrangement for x-ray astronomy ($E \lesssim 10$ keV) is shown in Fig. 2e. The x-rays reflect off a very shiny surface that looks like the inside of a cylinder but in reality has a parabolic shape in cross section, a paraboloid. This form will focus perfectly a point source at great distance that is on the axis of the paraboloid, but will not focus well objects that are off the axis. In the most elegant systems, the x rays reflect twice from the inner surface, first from a parabolic surface and then from a hyperbolic surface (Fig. 2f). This provides good off-axis focusing.

The grazing geometry yields a relatively small collecting area since the photons must strike the inclined surface of the mirror. To improve the collecting area, a number of mirrors can be nested within one another; a second such mirror is shown in Fig. 2e. Some x-ray systems emphasize large collecting area rather than high angular resolution. They have conical mirrors that approximate the parabolic shape and have dozens of such mirrors nested about a common axis.

Non-focusing systems

Electromagnetic radiation with photon energies above $\sim$10 keV (e.g., high-energy x rays and gamma rays) can not be focused with currently known techniques. Thus alternative non-focusing methods of constructing images are used. Although generally non-focusing systems are much less sensitive to faint sources, they are sometimes preferred even when focusing is available. For example, in the 1–10 keV band, the study of time variability of bright sources requires large collecting areas which are difficult to attain with x-ray focusing systems. The Rossi X-ray Timing Explorer (RXTE, launched 1995) uses such techniques to study black hole and neutron star systems.

Tubular and modulation collimators

Mechanical collimators may be used to restrict the regions of the sky that their detectors can "see". One type is simply a set of stacked tubes, like handfuls of soda straws (Fig. 3a). Since the radiation from a particular point on the sky impinges on the entire detector, the signal from the star must contend with background from the entire detector. The range of angles $\Delta\theta$ from which photons can reach a point on the detector through a tubular collimator is shown in Fig. 3a (inset); $\Delta\theta \approx d/h$.

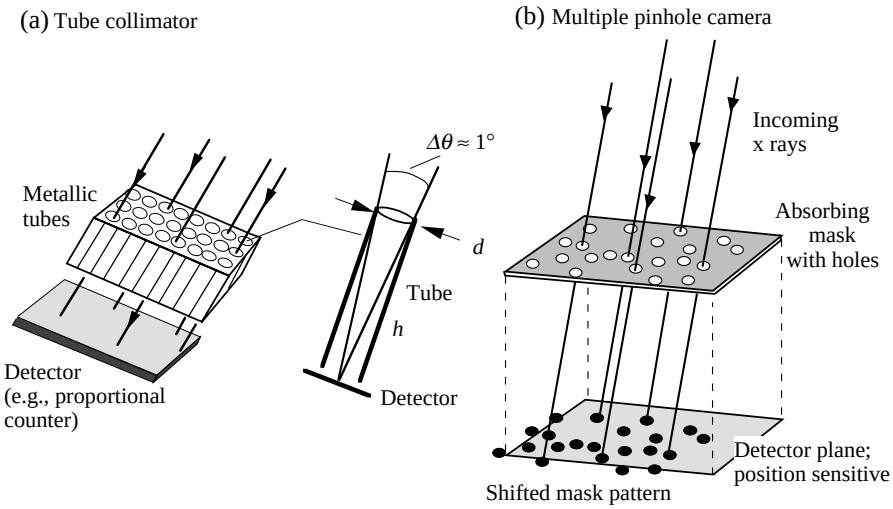

Figure 5.3. Non-focusing collimation. (a) Mechanical tubular collimation ("soda straws") and an expanded view of one of the tubes showing the angular extent of the field of view. (b) Operation of a multi-pinhole camera. The location of the shifted image of the mask pattern reveals the arrival direction of the photons.

This opening angle is comparable to the angular resolution. The angular resolution attainable with tubular collimators is typically $\sim 1^\circ$. The detector used with such collimators is likely to be a *proportional counter* or a *crystal scintillator* (Sections 6.2 and 6.4).

Tubular collimators make possible x-ray or gamma-ray systems with larger apertures than focusing telescopes, albeit at the expense of angular resolution. Timing studies of bright x-ray sources are made possible by the large aperture because large numbers of detected photons are needed to provide the required statistical precision in short time intervals. The detectors need not be *position sensitive*; the detector output does not distinguish where on the detector the photon landed. It is the mechanical collimator that defines the arrival direction of the incoming rays.

Multiple pinhole collimator

If one uses a detector that locates the position at which a photon strikes its surface, such as a piece of film, or a CCD detector (Section 6.3), other arrangements become possible. For example, a mask with randomly placed "pinholes" may be placed above the detector. A point source will then project a pattern of pinhole images onto the detector (Fig. 3b). The sideward displacement of the pattern on the detector surface directly indicates the direction from which the photons arrived, i.e., the location of the source on the sky. This is an extension of the simple pinhole camera from one to many pinholes. The multiple pinholes provide more effective area,

but they introduce more interference between the patterns if there are two or more sources in the field of view (FOV). A typical system would have a large FOV, say 30°. The angular resolution is much less, say $10'$, because it derives from the (small) pinhole diameter and the (large) distance between the mask and detector.

The existence and location of multiple point sources in the FOV of such a system can be deduced by searching the data mathematically for the multiple mask patterns. At each point x,y on the detector surface, there is an accumulated or recorded number of photons. Subtract a constant from all the values to force the average over all x,y to be zero. That constant will, of course, be the average of the original numbers. The result is a function that varies with x,y and takes on positive and negative values from pixel to pixel. Call this the response, $R(x,y)$; it is the real data. Now, compare this to the response $R_\mathrm{p}(\alpha,\delta,x,y)$ expected at x,y for a single hypothetical point source at some arbitrary sky position α,δ, and similarly adjusted to zero average. This is a trial function. This comparison is accomplished with the *cross-correlation function* (CCF), $\mathrm{C}(\alpha,\delta)$,

$$C(\alpha,\delta) \equiv \iint_{\substack{\text{All } x,y \text{ in} \\ \text{plane of detector}}} R(x,y)R_\mathrm{p}(\alpha,\delta,x,y)\,\mathrm{d}x\ \mathrm{d}y \tag{5.5}$$

(Cross-correlation function, CCF)

If one had chosen the response function for the position α,δ where a source really exists, and if that source were the only one in the field of view, the two functions R and R_p would be identical at all points x,y, except for statistical fluctuations in the real data. When one is positive, the other would also be positive, and similarly for the negative excursions. Thus, at all points, their product would be positive, and the sum (integral) of the product over the detector plane would then yield a large positive number. If on the other hand, there is no source at the chosen position, the two functions (trial and real) will differ more or less randomly with respect to one another. The products will be both randomly positive and negative, and the result of the integration will be approximately zero.

Calculation of $C(\alpha,\delta)$ for all trial positions (α,δ) in the field of view would thus yield only one position (resolution element) with a high value. All other positions would yield near-zero correlations. A sky map could be constructed with the values of $C(\alpha,\delta)$. It would show a high spot at the position α,δ of the actual source.

This technique can be used even if several celestial sources are in the field of view; the CCF map will reveal them. Each will appear as a bump in the map roughly proportional to its intensity. The net result is a pseudo or reconstructed image of the sky. The map may contain *side lobes* and other bumps or features that are not in the real sky because the mask patterns are not perfectly random. Thus one must

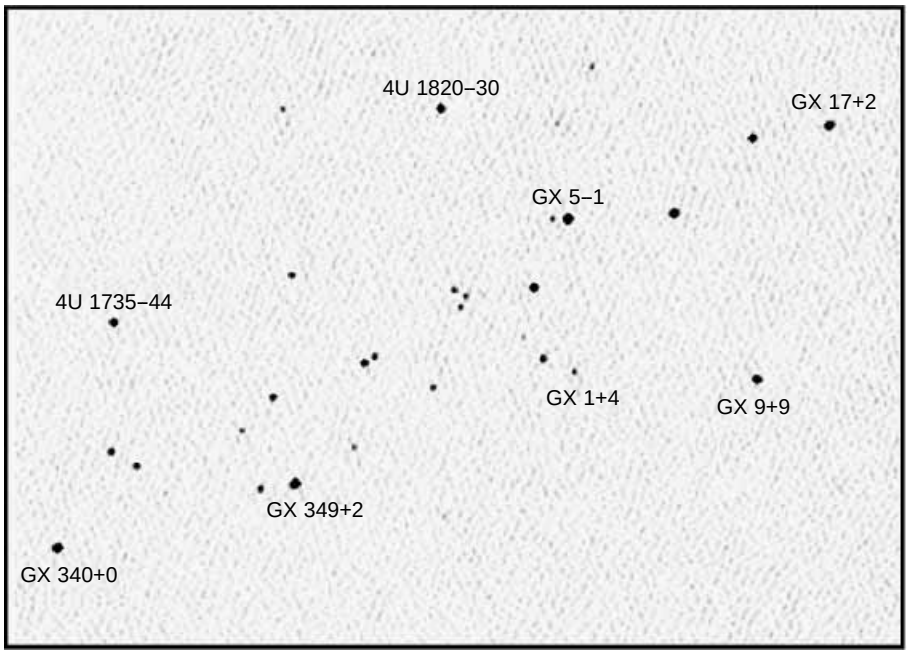

Figure 5.4. Reconstructed "image" of x-ray sources in the galactic center region, obtained with the wide field camera (WFC) multiple-pinhole instrument on the Italian–Dutch BeppoSAX satellite (launched 1996). The $\sim$30 x-ray sources above threshold lie along about 40° of the galactic plane. The GX source names are in galactic coordinates (degrees) while the 4U names are in celestial coordinates. [From J. In't Zand, *Proc. 4th Integral Workshop; ESA-SP*, astro-ph/0104299]

take care not to believe everything one sees in such a map, or in data of any kind. (See Section 7.3 for map cleaning algorithms.)

A French experiment Sigma on the Russian satellite Granat and the Dutch Wide Field Camera (WFC) on the Italian BeppoSAX satellite were pinhole cameras that imaged the x-ray sky at photon energies of 2–30 keV. Since many of these sources are variable in intensity, successive exposures permitted the intensities to be monitored on extended time scales. A reconstructed image of the galactic center region from the WFC is shown in Fig. 4.

Although such systems can yield sky maps including a number of discrete sources, they do not provide true imaging. Unlike focusing systems, the signal from a given point source illuminates the entire counter and hence must contend with the background from the entire detector as well as with the flux from all the other sources in the field of view. These both contribute to the background noise. Such systems generally yield angular resolutions down to a few arcminutes whereas focusing systems yield resolutions of $\lesssim 1''$ in the optical and x ray.

Some real telescopes

Most radio astronomy is ground based, e.g., the new (in 2000) steerable-dish 100-m diameter Byrd Green Bank Telescope in West Virginia, the huge (300-m) fixed antenna dish in Arecibo, Puerto Rico, and the cooperative world-wide collection of diverse telescopes that work in concert to obtain extremely high angular resolutions, called *very long baseline interferometry* (VLBI; Section 7.4). Radio astronomy from space can extend our knowledge of the radio sky to frequencies below the ionospheric cutoff at $\sim$10 MHz. Ideally this would be carried out with telescopes on the far side of the moon to eliminate radio noise from the earth. Observations from orbiting satellites can improve the angular precision of VLBI measurements. The Japanese HALCA satellite, launched in 1997, carried out VLBI in conjunction with ground-based telescopes, and a successor mission is being planned.

At microwave frequencies, the Cosmic Background Explorer (COBE) satellite (1989–93) studied the residual radiation from the hot early universe and established with greatly increased confidence that it did in fact originate in the early universe. It also found tiny fluctuations in its brightness that are most likely the origins of galaxy formation. Recent followup studies of these fluctuations with, for example, the Wilkinson Microwave Anisotropy Probe (WMAP, 2001) yield improved values for parameters that describe the universe, such as the Hubble constant. The Submillimeter Wave Astronomy Satellite (SWAS, 1998) studies star formation; it maps the location of spectral lines from molecules such as H_2O and O_2 in *giant molecular clouds* and *dark cloud cores* at frequencies near 500 GHz. The Submillimeter Array is an array of eight 6-m telescopes being built on Mauna Kea in Hawaii that will reach to 900 GHz with angular resolutions as fine as $0.1''$.

In the infrared, the ground-based all-sky survey at wavelength 2 μm (2MASS) has greatly expanded our knowledge of the IR sky. The orbiting Infrared Astronomical Satellite (IRAS, 1983) had previously surveyed the sky at 12, 25, 60, and 100 μm, and studies of these sources were the objective of the European Infrared Space Observatory (ISO, 1995–1998). Infrared radiation passes through interstellar clouds of gas and dust much more easily than does optical radiation. Thus IR astronomers can peer into dusty regions where stars are currently being formed. A major infrared satellite mission is the Space Infrared Telescope Facility (SIRTF, scheduled for 2003).

At optical wavelengths, a number of large ($\sim$10-m diameter) ground-based optical telescopes with new capabilities are now operational or coming on line, e.g., the Keck twin telescopes on Hawaii, the Gemini twin telescopes in Hawaii and Chile, the twin Magellan telescopes in Chile, the European quadruple Very Large Telescope in Chile, and the Japanese Subaru Telescope in Hawaii. In space, the

Hubble Space Telescope (HST, 1990), being above the atmosphere, provides resolution of about $0.05''$. The more finely focused images enable it to detect fainter and more distant objects than heretofore possible. *Speckle interferometry* and *adaptive optics* are new techniques coming into use to overcome the atmospheric blurring for ground-based telescopes, at least for some observations (see below). The use of multiple telescopes at one site enables optical astronomers to use *optical interferometry* to greatly improve angular resolutions (Section 7.4), at least for bright sources.

The orbiting International Ultraviolet Explorer (IUE, 1978) was sensitive over the range 3.8–10.8 eV (320–115 nm). The HST, although primarily an optical telescope, is sensitive from the near-IR up into the UV band: $E = 1.1$–10.8 eV ($\lambda = 1100$–115 nm). The important Lyman-alpha transition of hydrogen at 10.2 eV (see Fig. 10.1) is accessible to the HST. Spectroscopy in the far UV is being carried out by the Far Ultraviolet Spectroscopic Explorer (FUSE, 1999, 10.3–13.8 eV, 120–90 nm) which studies the spectral lines of atoms in the diffuse gases of the interstellar medium, supernova remnants, and other galaxies. At higher photon energies, beyond the 13.6 ionization energy of hydrogen which makes the ISM quite opaque, the Extreme Ultraviolet Explorer (EUVE, 1992–2000) studied nearby isolated hot white dwarfs, white dwarfs in accreting binary systems (cataclysmic variables), and the local hot interstellar medium itself.

The Uhuru satellite (1970) was the first orbiting satellite dedicated solely to celestial x-ray astronomy; it demonstrated the existence of neutron stars in binary stellar systems. It was followed by a succession of primarily US, European, and Japanese satellite missions that extended the field into a major branch of astronomy with imaging, spectroscopic, and timing capabilities. Current or recent missions include the German Roentgen satellite ROSAT (1990), the Japanese ASCA (1993), the US Rossi X-ray Timing Explorer (1995), and the Italian and Dutch BeppoSAX (1996). More recently launched (1999) are the powerful US Chandra and the European XMM–Newton observatories. They are large x-ray telescopes with reflective optics that focus x rays, yielding images and spectroscopy of distant objects with unprecedented sensitivity.

Gamma-ray astronomy has been carried out from space with a series of satellites leading up to the recent Compton Gamma-Ray Observatory (CGRO) which studied *gamma-ray bursts* (GRB) extensively. The recently launched Integral and the forthcoming SWIFT and GLAST missions will carry on the field. A major breakthrough in gamma-ray astronomy has been the determination that the explosive GRB take place in distant galaxies and hence are the most energetic explosions known, except for the Big Bang origin of the universe.

At energies beyond about 10^{12} eV, the field is called TeV astronomy or VHE (Very High Energy) astronomy. The fluxes of such energetic gamma rays are so

low that detections by a satellite would be rare. However, the gamma rays of these energies develop in the atmosphere into a cascade of electrons and lower energy gamma rays, known as an *extensive air shower* (EAS; Section 12.3). The electrons emit light in the atmosphere (Cerenkov light; Section 12.2) that can be seen from ground level with big crudely-focusing (by optical-astronomy standards) light-collecting telescopes. Some dozen sources have been detected, primarily galactic pulsars, supernova remnants and jets in extragalactic *blazars* (the nuclei of very active galaxies). This astronomy has been carried out with ground-based telescopes, e.g., in Arizona and the Canary Islands at the Whipple and HEGRA observatories, respectively. Although the number of detected sources is few and the angular resolution modest, the processes studied are among the most energetic in astronomy. New more powerful facilities coming on line over the next few years are HESS (European), CANGAROO III (Australian), and VERITAS (US).

Gamma-ray astronomy above $\sim 10^{14}$ eV is carried out through detections of electrons in the gamma-ray initiated EAS that reach ground level. To date, no verified signals from point sources have been detected in this energy range. The high background due to EAS initiated by the more numerous incident protons mitigates against such detections.

5.4 Antenna beams

Meaning of a "beam"

The concept of an *antenna beam* is intrinsic to all astronomy. The beam is simply the portion of the sky observed by the detector at a given time (Fig. 5). For example, in a non-focusing detection system, mechanical collimators might restrict the *field-of-view* to a circular region on the sky of 0.7° radius. The detector would be said to have a 0.7° beam (half width) or 1.4° (full width) that views $\sim \pi(0.7)^2 = 1.5$ deg^2 of the sky.

A parabolic radio antenna is a classic example of a focusing system. If this antenna were broadcasting (rather than receiving), the power would be emitted more or less into a cone of angles, the antenna beam, with the power per unit solid angle at a maximum on the view axis and falling off at increasing angles from it. The power would not be emitted in a perfectly parallel beam (i.e., to a point at infinity). This is due to the phenomenon of diffraction that arises from the limited diameter of the antenna.

The same antenna in the receiving mode receives radiation from this same cone of angles; any celestial source within it would be detected, with efficiency (sensitivity) depending on the source location relative to the view axis. If several point-like sources lie in this region, they would be confused or "unresolved" (Fig. 5a). The

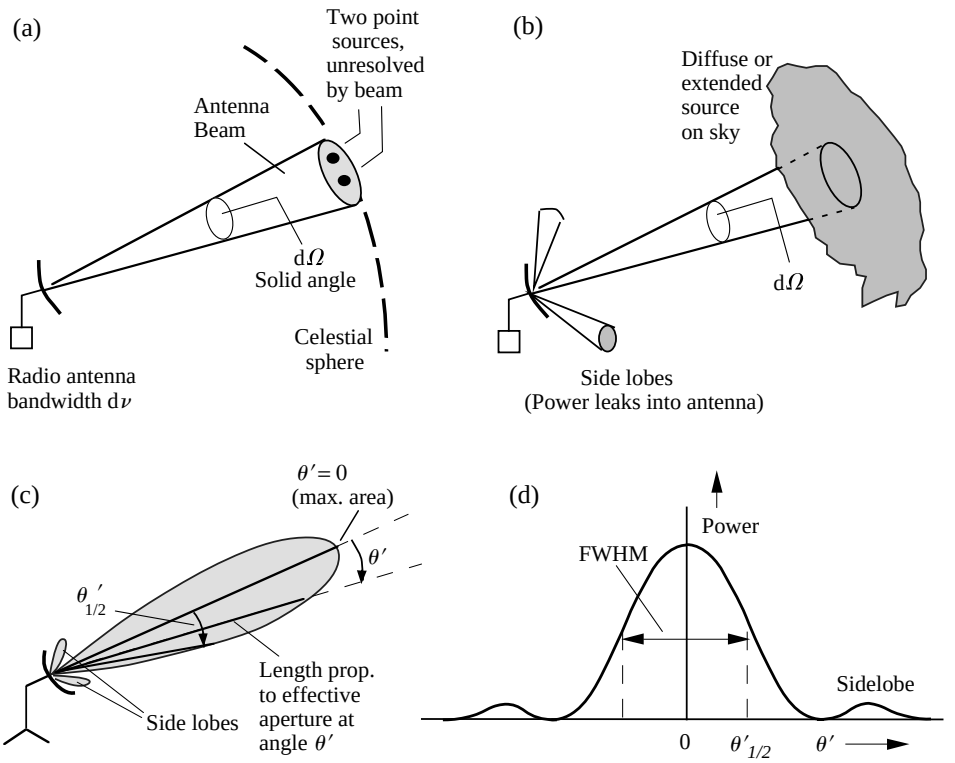

Figure 5.5. Antenna observing (a) two adjacent point sources that are not separated (resolved) by the beam and (b) a diffuse source that has greater angular extent than the beam. The beam includes side lobes wherein small amounts of power from unwanted directions can enter the receiver. (c) Power diagram; the beam is drawn so that the radial distance from the origin (antenna) to the solid line represents the effective sensitivity or area of the telescope in that direction. (d) Power received by the telescope as a function of the angular displacement of the source θ' from the telescope center line. The full width between the half-power points is the full width at half maximum (FWHM) beam size, or equivalently, the half power beam width (HPBW).

angular resolution of the telescope system is comparable to the angular size of the beam.

Each small portion (resolution element) of the film or CCD in a camera can be thought of as a detector that views, say, a $1'' \times 1''$ portion of the sky. Adjacent elements view adjacent portions of the sky. Thus a camera or focusing telescope is in effect a multiple-beam instrument. Such an imaging system is able to record the signal coming from different sky positions simultaneously, whereas a single-beam system must study adjacent portions of the sky sequentially. Examples of single-beam systems are the parabolic radio antenna with a single detector at the focus

and an optical telescope with a single small hole in the focal plane. In the latter case, all the light from the star of interest passes through the hole and the photon number may be measured with an electronic device called a photomultiplier tube which we describe in Section 6.2; see Fig. 6.1.

Point spread function

When a beam has a small angular size, closely spaced sources can be better resolved. Even if only one source is in the region, a narrow beam gives less contamination from background radiation from directions adjacent to the source. On the other hand, a broader beam is more efficient if one is searching a large portion of sky for sources or if one is studying diffuse radiation from the sky. However, it might confuse or wash-out bright spots in the emission pattern.

At the focus of a telescope, the beam size is the portion of sky that one single pixel in the focal plane can "see". Blurring by the telescope, the atmosphere, or by diffraction means that a faint point-like source will appear as a blurred (enlarged) image in the focal plane. Pixels in this region thus detect photons from the source even though they are not at the exact image position of the point source. Each pixel thus sees a larger portion of the sky than it would in the absence of blurring; the beam of each pixel, and hence of the telescope, is thus increased by any blurring (defocusing). In an optical telescope at ground level, this blurring may be primarily due to variable refraction in the atmosphere. (Diffraction is more important only for the smallest telescopes; see below.) Typically atmospheric blurring of $1''$ means the telescope beam size is effectively $1''$.

The analysis of images of the sky requires knowledge of the response of the telescope to a point source, in particular the x,y distribution of deposited energy in the image plane. This is a two-dimensional function $f(x,y)$, the *point spread function* (psf). This multi-pixel image maps the single-pixel beam shape.

A typical psf will be peaked in the center with the deposited energy falling off with distance. For modestly bright objects recorded on photographic film, the film saturates; it reaches maximum blackness at the center of the image. But light scattering on the film surface enlarges the exposed region. Thus on photographs of the sky, the brighter stars appear bigger, not brighter. The psf in this case is flat and broad; the effective beam is larger for the brighter sources.

The number of photons collected (in a given time) is a strong function of the angular position of the source relative to the center of the beam as noted above. The effective area of a telescope is different for different parts of the antenna beam; an object directly on the axis of a radio telescope will deliver more of its energy to the focus than will an off-center one. Sometimes, a source far off to the side can be weakly detected if the beam has undesirable *side lobes* (Figs. 5b,c). A strong source in a side lobe will be indistinguishable from a weak source in the main beam.

An antenna beam can be drawn as shown in Fig. 5c. The radial distance from the origin (antenna) to the lobe boundary at a chosen angle is proportional to the effective area of the antenna for radiation arriving from that angle. Typically, the greatest efficiency is in the forward direction.

The quoted angular width of the beam depends on how the edge is defined. A definition often used is the *full width half maximum* (FWHM; Fig. 5d). If $\theta_{1/2}{}'$ is the angle from beam center at which the power is reduced to $1/2$ its maximum value, the FWHM angle is $2\theta_{1/2}{}'$. Radio astronomers refer to this as the *half-power beam width* response (HPBW). Although the power received at $\theta_{1/2}{}'$ is $1/2$ the power in the center of the beam, the total power *enclosed* within this angle can be substantially greater than (or less than) 50% of the total power over all angles.

A good telescope beam will have a highly peaked response function which will include $\gtrsim$90% of the received power within the FWHM limits, but a poor beam can have a response with large "wings" that result in only a small portion of the power falling within the FWHM angles. Another useful definition of beam width is the (half or full) angle that encloses 90% of the power. A beam with large wings would have a large value of this angle and vice versa.

Diffraction

One reason a telescope beam may not be as narrow as one might wish is an interference phenomenon known as *diffraction*. If a parallel beam from an infinitely distant source is incident upon an antenna, there is interference between the different parts of the incoming wavefront, called *wavelets* in the Huygen method of describing wave propagation. If the telescope has a limited diameter (i.e., it is not infinitely large), the interference will produce a blurred (enlarged) image of size that depends upon the diameter of the telescope.

Fraunhofer diffraction

A formal derivation of diffraction sums the effect of wavelets originating at each imaginary segment of an aperture such as that shown in Fig. 6a. The aperture could be the aperture of the primary mirror of a telescope. The wavelets are in phase at the aperture if they originate in a plane wave. They interfere with one another as they propagate downward from the aperture. The resultant propagation directions deviate from the vertical because the blocked parts of the original wavefront are missing.

Fraunhofer diffraction is the special case of diffraction where the distance to the image plane is large compared to the diameter d of the aperture. A segment of a plane wave of light leaving the aperture at a given angle θ (Fig. 6b) thus will illuminate one part of the distant image plane, and the light leaving at a different angle will illuminate another portion. In this manner, two stars will appear as two spots on the distant focal plane. Alternatively, one could insert a thin lens just below

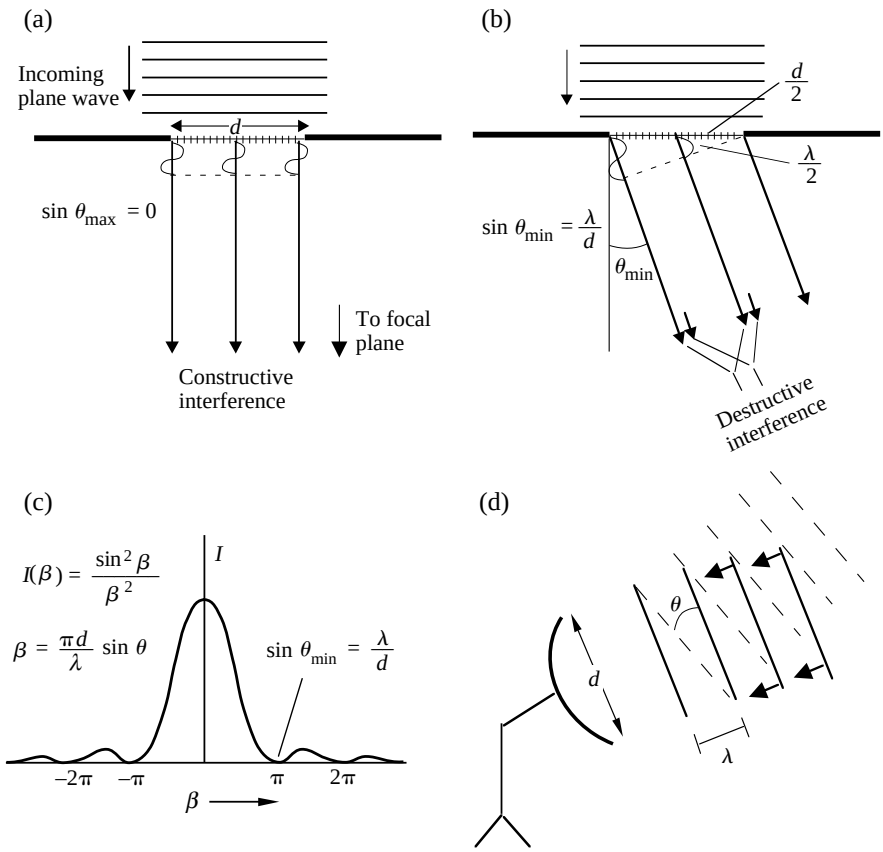

Figure 5.6. Fraunhofer diffraction of an incoming parallel beam by a single slit viewed from its short end. The slit is imagined to consist of the multiple segments shown. The image plane is taken to be at a very large (infinite) distance downward. (a) Forward direction ($\theta = 0$) wherein the wavelets from all segments are in phase giving maximum intensity. (b) Direction θ defined by $\sin\theta = \lambda/d$, in which the summed wavelets yield zero intensity, the first minimum of the response. (c) The one-dimensional response function, intensity vs. $\beta(\theta)$. (d) The half angle of diffraction smearing $\theta_{\min} \approx \lambda/d$ represents an uncertainty in the arrival direction that is equivalent to the wavefront arriving at the telescope aperture with one edge lagging the other by one wavelength.

the aperture to bring the rays at each angle to a focus on a nearby focal plane. This simply moves the image plane closer and is the arrangement of a typical telescope.

In either of these cases (with and without a lens), for each angle θ, one can examine the interference of the wavelets from imaginary segments of the aperture. The simplest geometry to consider is an aperture which is a long, narrow slit (running into and out of the paper) of width d. Figures 6a,b show the narrow dimension of the slit. At the angle $\sin\theta = \lambda/d$ (Fig. 6b), the rays from the left and center of

the aperture are perfectly out of phase because the path length difference is exactly $\lambda/2$. The rays from the segments just to the right of these (shown as short arrows in Fig. 6b) also are perfectly out of phase with each other for the same reason. In fact, each pair of segments in the left half of the slit has a partner in the right half which exactly cancels the first. Thus, one would expect no light at this particular angle,

$$\sin\theta_{\min} = \frac{\lambda}{d} \qquad \text{(Angle of destructive interference; slit interference)} \tag{5.6}$$

In contrast, the rays directed straight ahead at $\theta = 0$ (Fig. 6a) are all in constructive interference.

A proper summation of the phases and amplitudes of all the wavelets over the narrow slit for each angle θ leads to an intensity pattern of the form,

$$I(\beta) = \frac{\sin^2\beta}{\beta^2} \qquad \left(\beta = \frac{\pi d}{\lambda}\sin\theta\right) \qquad \text{(Fraunhofer slit diffraction)} \tag{5.7}$$

This function (Fig. 6c) has a maximum value of 1.0 at $\beta = 0$, or $\theta = 0$. It has minima with zero value when $\sin\beta = 0$, i.e., at $\beta = \pm n\pi$, where n is an integer ≥ 1. The first minimum at $\beta = \pi$ corresponds to the angle $\sin\theta_{\min} = \lambda/d$ shown in Fig. 6b. The second minimum is at $\beta = 2\pi$, or $\sin\theta_{\min} = 2\lambda/d$. Thus the minima will generally be separated by $\Delta\theta \approx \lambda/d$ for small angles, $\theta \ll 1$ so that $\sin\theta \approx \theta$. The two central minima are an exception; they are separated by twice this amount.

The circular aperture of a telescope mirror yields a circular diffraction pattern as expected from the symmetry. Again, a proper summation of the wavelets must be carried out to obtain the radial variation of brightness. The result is similar in form to Fig. 6c. It turns out that the angular radius $\theta_{\min}$ of the first minimum (dark ring), which encircles most of the light, for $\lambda \ll d$, is

$$\theta_{\min} \approx 1.22\frac{\lambda}{d} \qquad \text{(rad; circular aperture; } \lambda \ll d\text{)} \tag{5.8}$$

where λ is the wavelength of the incoming radiation and d is the diameter of the mirror or antenna. A sketch of the appearance is presented in Fig. 7. This is called the *Airy diffraction pattern*, and the inner part, within $\theta_{\min}$ is called the Airy disk.

The diffraction phenomenon is equivalent to saying that the antenna can not distinguish the arrival directions that lie within angles $\theta_{\min} \approx \lambda/d$ of the source directions; the two sources can not be resolved if they are closer together than this angle. (Even so, with sufficient signal, the response will be broadened or asymmetric, possibly revealing the presence of the second source.) As shown in Fig. 6d, the angle $\theta_{\min}$ corresponds to a shift of phase of only one wavelength across